JOURNAL OF THERMOPHYSICS AND HEAT TRANSFER
Vol. 6, No. 4, Oct.–Dec. 1992

Thermal Control Coatings Performance at Near Geosynchronous Altitude

D. F. Hall* and A. A. Fote†
The Aerospace Corporation, Los Angeles, California 90009

Flight measurements on 16 spacecraft thermal control coating materials over 10 yr at geosynchronous altitude are reported. Fused-silica second-surface mirrors and polished metals are essentially stable in space; observed increases in solar absorptance <0.002/yr are ascribed to contamination. Metalized Teflon® FEP and aluminized Kapton® darken over a long period of time. Two types of conductive mirror coatings darken measurably. The backing material on Astroquartz fabrics influenced their darkening. The time dependence of the darkening of these samples is well described by physical models of the degradation processes. 3M 401C10 black paint and Grafoil samples lighten over a long time period. NASA/GSFC NS43G conductive yellow paint darkens over a long time period.

Introduction

THERMAL control coatings (TCCs) are used onboard spacecraft to reflect solar radiation and to emit component heat so that temperature limits are not exceeded. Unfortunately, TCCs degrade with time on orbit. In high Earth orbit at least three processes can produce changes in their thermooptic properties: the materials can 1) adsorb contaminants outgassed by other parts of the spacecraft; 2) suffer damage from natural radiation (photons, protons, electrons); and 3) deteriorate as a result of vacuum exposure and temperature cycling. Reliable information concerning the causes and rates of TCC degradation has been hard to obtain with ground-based measurements because it is not clear which aspects of the space environment must be accurately simulated, and because of the problem of facility-induced contamination. Generally, in previous flight measurements of TCC degradation, contamination from the host vehicle has also been an important, but unquantified factor. The ML12 space experiment was designed to minimize contamination effects and to increase understanding of the other processes. We report flight measurements on 16 thermal control coating materials made during 10 yr near geosynchronous altitude.

Experimental Details and Results

P78-2 Spacecraft

The P78-2 spacecraft is managed and funded by the United States Air Force (USAF) Space Test Program. It was one element of a cooperative National Aeronautics and Space Administration (NASA)/USAF program to investigate various aspects of the electrical charging and discharging of geosynchronous spacecraft surfaces (Refs. 1 and 2). The program is known as SCATHA (Spacecraft Charging At High Altitudes).

The P78-2 was launched on January 30, 1979, into a 176- by 43,278-km transfer orbit. On February 2, it was injected into a 27,578- by 43,228-km, 7.9-deg inclination final orbit. The vehicle, pictured in Fig. 1, is a right cylinder approximately 1.75 m in both length and diameter.

The objectives of P78-2 were to measure 1) the environments that lead to charging; 2) the characteristics of the vehicle plasma sheath; and 3) the effects of charging on vehicle subsystems. To achieve these objectives, it carries a complement of six charged-particle experiments, electron and positive ion emitters, magnetic and electric plasma field detectors, satellite surface potential monitors, and instruments to characterize electrical discharges, and the contamination experiment (Ref. 2).

Contamination Experiment

Two sensor types are used. One type is a combination retarding potential analyzer (RPA) and temperature-controlled quartz crystal microbalance (TQCM). With it, distinction can be made between charged and uncharged arriving molecules, and information can be obtained concerning the temperature dependence of the contaminant absorption and desorption rates. The other sensor type exposes samples of various spacecraft thermal control coatings (TCCs) to the natural environment and arriving contaminants, and continuously measures the solar absorptances (α_s) of these samples (Ref. 3).

As shown in Fig. 1, there are two of each type of sensor on the satellite. Both of the TCC trays and one of the RPA/TQCMs view radially. The other RPA/TQCM views axially from the "forward" end of the space vehicle. The three sensors mounted on the vehicle belly band between the SC2 and SC11 booms have nearly clear fields of view. The fourth sensor, mounted flush with the forward end of the vehicle, has a portion of the main communication antenna within its field of view. This document focuses on data from the TCC trays; Refs. 4 and 5 contain discussions of RPA/TQCM results.

TCC Experiment

The TCC instrument package consists of two sample trays (one shown in Fig. 2) that carry eight 1.25-in.-diam samples

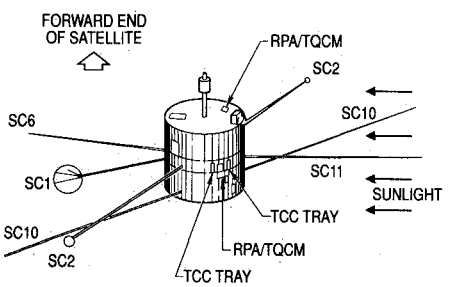

Fig. 1 P78-2 spacecraft.

Presented as Paper 91-1325 at the AIAA 26th Thermophysics Conference, Honolulu, HI, June 24–26, 1991; received July 25, 1991; revision received Nov. 20, 1991; accepted for publication Nov. 21, 1991.

*Research Scientist, Surface Science Department, P. O. Box 92957. Member AIAA.

†Member of the Technical Staff, Solid State Electronics Department, P. O. Box 92957.

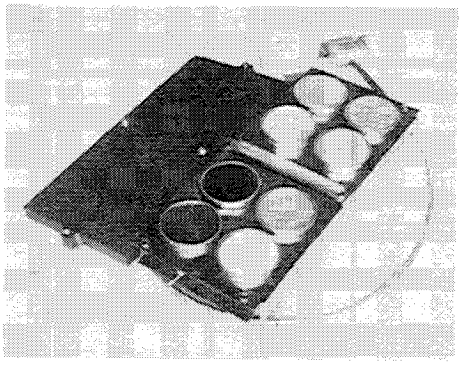

Fig. 2 Photograph of TCC tray.

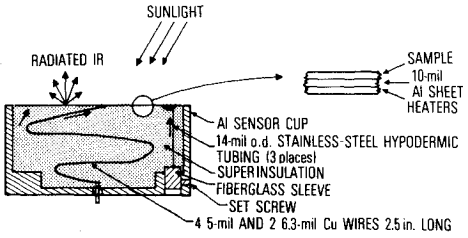

Fig. 3 Cross section of TCC sample mounting.

Table 1 Flight samples

ML12-3 Tray	ML12-4 Tray
Grafoil (Union Carbide, GTA grade)	10-nm Au on 5-mil Kapton[b]/Al (Sheldahl Lot 105788 coated by SRI)
Black paint (3M401C10)	Astroquartz silica fabric (J. P. Stevens 581)/FEP/Al
Fused-silica mirror (OCLI[a] SI-100)	Conductivity coated fused-silica mirror (OCLI)
Vacuum-deposited Au (optically opaque) on Al	22-nm 10% SnO_2, In_2O_3 on 2-mil Kapton/Al (prepared by G.E.)
Diamond-polished 2024 T3 Al	Diamond-polished 2024 T3 Al
Teflon[b] FEP (2 mil)/Ag (Sheldahl[c])	Black paint (3M401C10)
Teflon FEP (5 mil)/Ag (Sheldahl)	Astroquartz silica fabric (J. P. Stevens 581)/tape (Sheldahl 405900)
Yellow paint (NASA-Goddard No. NS43G)	Kapton (5 mil)/Al (Shendahl)

[a]Optical Coating Laboratory, Inc., Santa Rosa, CA 95402.
[b]Trademark for E. I. DuPont de Nemours.
[c]Sheldahl, Inc., Northfield, MN 55057.

each and the electronics required to monitor the sample temperatures (Refs. 6 and 7). Thermal isolation of the samples from the tray resulted in conduction and radiation coefficients of approximately 9×10^{-4} W/K and 7.9×10^{-12} W/K^4, respectively. These values are about average for flight calorimeters (Ref. 8).

The underside of each aluminum disk carries heaters and thermistors (see Fig. 3). The heaters are included for the purposes of preflight calibration and to allow thermal desorption cleaning of six of the samples on orbit. In addition, there are two thermistors located on each of the sample trays to measure the temperature of the supporting cups.

Samples include fused-silica mirrors, metallized polymers, polished metals, paints, and quartz fiber fabrics, as listed in Table 1.

Data Reduction

The solar absorptances of the samples are deduced from on-orbit measurements of temperatures and the prelaunch-measured values of thermal emittances and residual heat leaks (under the assumption that the values of thermal emittance measured before launch remain constant). This assumption is based on two facts: 1) the thermal emittance of these samples is insensitive to temperature over the range involved here; and 2) the thermal emittance property is far less sensitive to the presence of contaminant films than is the solar absorptance property, because the extinction coefficient of organic films in the infrared is much lower than in the visible.

Because the spacecraft rotates, the solar flux ϕ on the TCC samples varies according to

$$\begin{aligned} \Phi(t) &= 0 \qquad \text{for} \quad \pi \le \omega t \le 2\pi \\ \Phi(t) &= AE \sin \omega t \qquad \text{for} \quad 0 \le \omega t \le \pi \end{aligned} \tag{1}$$

where t = time, A = sample area, ω = angular velocity of spacecraft, and E = solar irradiance.

The heat balance equation is

$$C_v(T)\frac{dT}{dt} = F(T_c^4 - T^4) + C(T_c - T) + \varepsilon A\sigma(T_0^4 - T^4) + \alpha_s S\phi(t) + P \tag{2}$$

where T = sample temperature, T_c = tray temperature, T_0 = temperature of surroundings, F, C = thermal coupling constants between the sample and tray, $\varepsilon A\sigma$ = emissivity times sample area times Stefan-Boltzman constant, $C_v(t)$ = sample heat capacity, α_s = sample solar absorptance, S = factor between 0–1 to account for shading resulting from spacecraft booms, and P = power applied by means of sample heater.

Albedo and Earth emission are calculated to be nearly negligible at near synchronous altitude and are not included in Eq. (2). (Furthermore, from the second year on-orbit to January 1987, data reduction was limited to periods when the samples had no view of Earth.) Also neglected is the dependence of α_s upon the angle of incidence of the light. However, we have calculated the solar irradiance value E as a function of the time of year since this value varies ~7% as the Earth orbits the sun. The solution of Eq. (2) is discussed in Refs. 6 and 7.

Early orbital values of solar absorptance are (with the exception of one black paint sample) in good agreement with prelaunch values (Ref. 9) as shown in Table 2. For that sample, the early orbital value was 0.90 compared with 0.97 as measured prior to launch. The discrepancy is thought to be due to a problem in the flight sensor.

Prelaunch Calibrations and Calculations

The sample and tray thermistors were calibrated against precision copper constantan thermocouples in a temperature-

Table 2 Prelaunch values[a] of ε_H and α_S and first optical α_S

	Prelaunch measurement		Initial on orbit
	ε_H	α_s	α_s
Grafoil	0.34	0.66 ± 0.01	0.666 ± 0.001
Black paint (tray 3)	0.87	0.97 ± 0.01	0.90_3 ± 0.002
Fused-silica	0.81	0.08 ± 0.01	0.077 ± 0.0006
Gold	0.03	0.21 ± 0.01	0.191 ± 0.0006
Aluminum (tray 3)	0.05	0.1_4 ± 0.05	0.146 ± 0.0005
FEP (5 mil)	0.80	0.11 ± 0.01	0.11_5 ± 0.005
FEP (2 mil)	0.68	0.06 ± 0.01	0.07_0 ± 0.003
Goddard paint	0.78	0.31 ± 0.01	0.32_9 ± 0.003
Au film/Kapton	0.42	0.53 ± 0.01	0.52_8 ± 0.007
Fabric (FEP/Al)	0.68	0.20 ± 0.01	0.20_9 ± 0.003
Coated OSR	0.76	0.09 ± 0.01	0.07_8 ± 0.006
Coated Kapton	0.71	0.40 ± 0.01	0.39_6 ± 0.004
Aluminum (tray 4)	0.04	0.1_4 ± 0.05	0.140 ± 0.0009
Black paint (tray 4)	0.92	0.97 ± 0.01	0.962 ± 0.001
Fabric (tape)	0.60	0.19 ± 0.01	0.19_6 ± 0.005
Kapton	0.81	0.48 ± 0.01	0.51_1 ± 0.003

[a]Suppressed digits are not fully significant.

regulated oven/refrigerator. The determinations of C, F, εA, and C_v were performed in an ion-pumped vacuum chamber containing a black liquid-nitrogen-cooled shroud surrounding the trays. The trays were held in a temperature-controlled holder and kept near room temperature to duplicate the conditions expected on orbit. The thermal coupling constants C, F, and εA, were determined by applying a measured amount of power to the sample heaters and by measuring the equilibrium temperatures T and T_c. The values of ε, as determined by this procedure, are given in Table 2. Values of C and F for each sample were reported previously (Ref. 9).

To determine C_v, heater power was applied, and the data were recorded in the form of temperature vs time (30-s intervals), enabling the calculation of dT/dt for use in Eq. (2) (Ref. 9).

The shading factors S are a function of the angle ρ between the spacecraft spin axis and the sun, primarily because of one of the SC2 booms (see Fig. 1). Maximum shading occurs for the Grafoil and GSFC samples at $\rho = 90$ deg and represents a 10% drop in radiation. Values of S were calculated by Systems, Sciences, and Software, Inc., for $80 < \rho < 100$ deg in 1-deg steps for each of the 16 samples (Ref. 10). The samples are not shaded for ρ outside this range. In most cases in calculating α_s, we use telemetry data for time periods when ρ was such that shading did not occur.

Physical Models

The TCCs in Table 1 can be divided into "space-stable" and "nonspace-stable" categories. The space-stable TCCs are unlikely to degrade due to radiation, vacuum, or temperature cycling, but are subject to contamination. First-surface metal and second-surface fused-silica mirror samples are in this category. The nonspace-stable TCCs, which are subjected to all the degradation processes, include the remainder of the samples. The data on the space-stable samples reveal that contamination affects them much less than radiation damage and deterioration affect the nonspace-stable samples. (This is, in part, because of the low rate of contamination collection by the samples, which, in turn, results from their clear field view of space and the relatively high level of P78-2 cleanliness). For this reason, we ignore radiation effects when modeling the degradation of the space-stable samples, and ignore contamination effects when modeling the nonspace-stable samples.

Space-Stable Samples

As a general model, we imagine sunlight reflecting from a mirror consisting of two semitransparent layers of thicknesses x and y, and a metal surface of reflectance r. The top layer is assumed to be a uniform, continuous molecular film of contamination, with a solar spectrum weighted absorption coefficient, K. In the case of the OCLI SI-100 mirror sample, the second layer corresponds to fused-silica with absorption coefficient L. On the other hand, for the first-surface metal mirrors, $y = L = 0$

$$\alpha = 1 - r\exp(-2Kx - 2Ly) \tag{3}$$

Assuming the metal surface reflectivity to be constant

$$\frac{d\alpha}{dt} = 2(1-\alpha)\left(x\frac{dK}{dt} + K\frac{dx}{dt}\right) \tag{4}$$

Even after 10 yr, the contamination on the SCATHA spacecraft has been so low that the dependence of the solar absorptance of the space-stable samples on time appears linear, because the scatter in the data masks the rolloff that must be present. Therefore, for the purpose of curve fitting, Eq. (4) has been expressed as

$$\frac{d\alpha}{dt} = Q(1-\alpha) \tag{5}$$

where Q is a constant much less than unity. Then

$$\alpha = \alpha_0 + Qt \tag{6}$$

The quantitative results of a least-squares fit of this equation to the data of the four space-stable samples are given in Table 3 (in the first four entries). Also included are the standard deviations (Ref. 11) of the parameters and the standard errors (S.E.) (Ref. 12) of the fits. The data for the gold and one of the aluminum samples is plotted in Fig. 4. The uncoated fused-silica mirror data is plotted in Fig. 5 (along with the coated sample data to be discussed below).

It is seen that α increases very slowly for these samples, less than 0.002/yr. Since contamination is known to be accumulating on the nearby temperature-controlled quartz crystal microbalance (Ref. 5), we assert it is responsible for the increases observed. The rate of increase on gold is much smaller than for the other space-stable samples, for two reasons.

1) The gold sample has the highest temperature, and therefore transiently adsorbed molecules have a shorter time to photodeposit before desorbing again (Ref. 13).

2) α is already fairly high owing to its low spectral reflectance at wavelengths shorter than 600 nm. Spacecraft con-

Table 3 Eq. (6) Parameters for space-stable samples

	α_0	Q, day^{-1}	S.E.
Gold	0.1911 ± 0.0006	(2.0 ± 0.3)E-6	2.8E-4
Fused-silica	0.0768 ± 0.0006	(4.9 ± 0.3)E-6	2.7E-4
Aluminum (tray 3)	0.1456 ± 0.0005	(4.8 ± 0.3)E-6	2.7E-4
Aluminum (tray 4)	0.1400 ± 0.0009	(5.2 ± 0.4)E-6	4.1E-4
Black paint (tray 3)	0.903 ± 0.002	−(2.3 ± 0.4)E-3	1.0E-3
Black paint (tray 4)	0.962 ± 0.001	−(1.3 ± 0.2)E-3	5.9E-4
Grafoil	0.666 ± 0.001	(2.96 ± 0.08)E-5	4.8E-4

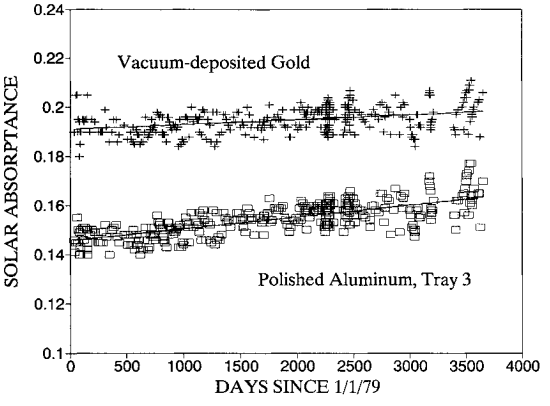

Fig. 4 Solar absorptance of vacuum-deposited gold sample and tray 3 polished aluminum sample vs time on orbit.

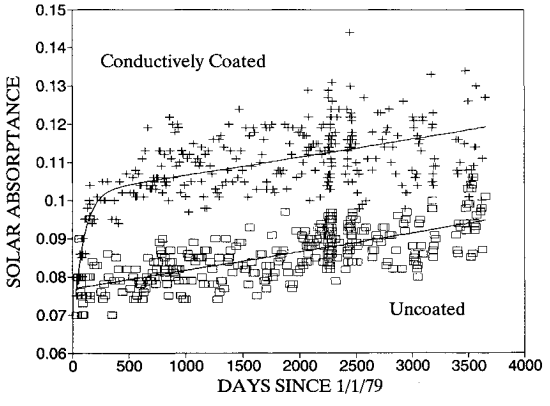

Fig. 5 Solar absorptance of fused-silica mirror and OCLI-coated fused-silica mirror samples vs time on orbit.

taminants typically have proportionately lower optical absorptance at wavelengths longer than this (Ref. 5). Thus, gold is less sensitive to α increases by contaminant layers than aluminum and silver, which have high reflectance well above 600 nm.

Non-Stable Samples

The degradation of the space-stable aluminum samples most likely represents the upper limit for the effects of contamination on the nonspace-stable, low solar absorptance samples. Since the latter samples exhibit much higher rates of degradation than the aluminum, we attribute their degradation to radiation damage, and ignore the relatively insignificant contribution from contamination. The quality of the agreement between this model, and the data, validates ignoring contamination of nonspace-stable samples.

While passing through the material of second-surface mirrors, the intensity of normally incident light suffers an incremental drop given by

$$dI = \pm K(x, t)I\, dx \tag{7}$$

where the negative sign applies during the inward path, and the positive sign applies during the outward path. The average solar spectrum weighted absorption coefficient is taken as an exponential function of both time and depth because of the effect of damage induced by natural radiation of finite penetration depth D. Specifically

$$K(x, t) = K_0 + f(t)\exp(-x/D) \tag{8}$$

where K_0 designates the absorption coefficient of the undamaged material, and $f(t)$ is the time dependence of the darkening of the affected region. Assuming a back surface reflectivity r and a total thickness of the material T, Eqs. (7) and (8) yield

$$1 - \alpha = (1 - \alpha_0)\exp\{-2f(t)D[1 - \exp(-T/D)]\} \tag{9}$$

Polymer Mirror Model

As first application of the general model, consider the second-surface polymer mirrors, specifically, the two silvered Teflon FEP and the uncoated aluminized Kapton samples.

The time dependence $f(t)$ of the polymer darkening is obtained from the assumption that specific sites in the material are susceptible to damage by radiation particles. Once hit by a particle, the sites are unaffected by subsequent particles. Thus, in time, the darkening reaches an equilibrium value, as is observed. If n is the fraction of susceptible sites that have been damaged, this process is described by

$$\frac{dn}{dt} = (1 - n)/\tau \tag{10}$$

where τ is the time constant for the process. Assuming that the absorption coefficient of the material is proportional to the density of damaged sites leads to

$$f(t) = f_f[1 - \exp(-t/\tau)] \tag{11}$$

where f_f is the saturation value of the absorption coefficient. This permits Eq. (9) to be written as

$$\alpha = 1 - \exp[A + B\exp(-t/\tau)] \tag{12}$$

where

$$A = \ln(1 - \alpha_0) - B \tag{13}$$

$$B = 2Df_f[1 - \exp(-T/D)] \tag{14}$$

Figure 6 displays the time dependence of the solar absorptances of the FEP samples. The 5-mil FEP sample data (otherwise similar to the 2-mil case) exhibits an anomalous decrease in α at 2455 days from January 1, 1979 (Ref. 9). This is due to irreversible damage to the sample holder on that day because of our exercising the heating element. Figure 7 displays the data for the uncoated Kapton sample (as well as of two coated samples to be discussed).

The "best-fit" parameters for the three samples to Eq. (12) are presented in Table 4. In the case of the 5-mil FEP sample, Eq. (12) was fitted using only the data prior to the event at 2455 days from January 1, 1979.

We notice that the values of the parameters "B" and "τ" differ for the two FEP samples. The fact that they differ, indicates a breakdown in the simplifying assumptions used to derive Eq. (12). Specifically, we assumed that τ was a constant throughout the thickness of the material. However, τ actually varies exponentially with depth because of the depth dependence of the radiation intensity. This effect becomes significant as the radiation damage approaches saturation.

Meanwhile, if we are less interested in theoretical modeling than in a descriptive equation, it turns out that, in regards to quality of fit, the following simpler equation fits just as well as Eq. (12):

$$\alpha = A + B\exp(-t/\tau) \tag{15}$$

The best-fit parameters in the case of Eq. (15) are also given in Table 4.

Gold-Coated Kapton

A more complex model (than the general model) is needed for the Kapton coated with a semitransparent gold layer. Because of multiple internal reflections off the gold coating and the second surface, we have shown (Ref. 7) that

$$\alpha_{Au/Kap} = 1 - \rho - (Cre)/(1 - \rho_{re}) \tag{16}$$

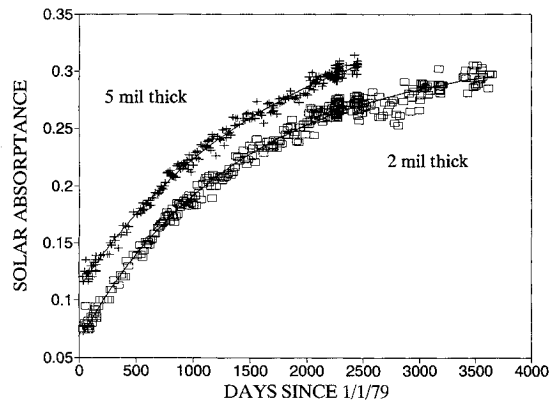

Fig. 6 Solar absorptance of 2-mil- and 5-mil-thick silvered Teflon FEP samples vs time on orbit.

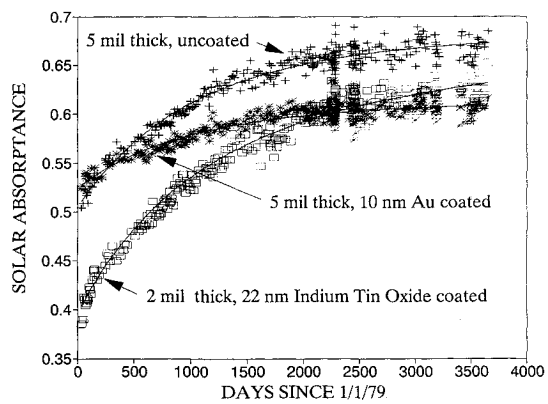

Fig. 7 Solar absorptance of uncoated, gold-coated, and ITO-coated aluminized Kapton samples vs time on orbit.

Table 4 Eq. (12) Parameters for polymer mirrors

	A	B	τ	S.E.
Kapton (Eq. 12)	−1.140 ± 0.006	0.437 ± 0.005	1240 ± 50	5.0E-4
2-mil FEP (Eq. 12)	−0.383 ± 0.003	0.318 ± 0.003	1600 ± 40	3.8E-4
5-mil FEP (Eq. 12)	−0.474 ± 0.007	0.357 ± 0.007	2070 ± 70	3.1E-4
Kapton (Eq. 15)	0.677 ± 0.002	−0.170 ± 0.002	1060 ± 37	4.9E-4
2-mil FEP (Eq. 15)	0.313 ± 0.002	−0.249 ± 0.002	1405 ± 30	3.7E-4
5-mil FEP (Eq. 15)	0.365 ± 0.004	−0.255 ± 0.003	1700 ± 50	3.1E-4

Table 5 Eq. (20) Parameters for the conductive coatings

	a	b	c	τ	S.E.
ITO	−0.100 ± 0.002	0.0041 ± 0.0003			7.5E-4
OCLI	0.0138 ± 0.0003		−0.021 ± 0.006	89 ± 26	2.4E-4

where $C = (1 - \rho)^2 \exp(-2Mz)$, $e = \exp(-2\{K_0T + f(t)D[1 - \exp(-T/D)]\})$ and z, M, and ρ refer to the thickness, absorption coefficient, and reflectance of the gold film, respectively. The simplifying assumption has been made that the same reflectance, ρ, applies for both the gold-vacuum and gold-Kapton interfaces.

The degradation of the gold-coated Kapton can be compared to that of the uncoated Kapton to see if they are caused by the same mechanism. Note that the uncoated Kapton can be described by Eq. (16) with $M = z = \rho = 0$:

$$1 - \alpha_u = re \tag{17}$$

Since r, D, K_0, and $f(t)$ should be the same for both the coated and uncoated samples, the following relation between the α's of these two should obtain

$$(1 - \alpha_c) = \rho + C\left[\frac{(1 - \alpha_u)}{1 - \rho(1 - \alpha_u)}\right] \tag{18}$$

Using Eq. (18) and the parameters of Table 4 for α_u, we obtain best-fit parameters between Eq. (18) and the α_u data to be $\rho = 0.246 \pm 0.004$ and $C = 0.407 \pm 0.01$. The S.E. is 4.3E-4. The data and Eq. (18) are plotted in Fig. 7.

The model, therefore, correctly predicts a relation between the α's of the coated and uncoated Kapton samples. It assumes a constant value for ρ, the reflectance of the gold coating, and M, its absorption coefficient, while including the same form of degradation for the Kapton itself. Therefore, the degradation of the gold-coated Kapton sample can be attributed exclusively to radiation damage in the Kapton. There is no evidence of degradation of the gold coating, nor is there evidence that the gold has shielded the Kapton from damage. The fact that approximately 25% of the visible light striking the gold is immediately reflected suggests that it is not an important contributor to the degradation of the Kapton.

Conductive Coatings

One of the Kapton (Fig. 7) and one of the fused-silica mirror (Fig. 5) samples carry a coating of conductive, nearly transparent material. The Kapton is coated with an indium-tin oxide (ITO) film, while the fused-silica is coated with an OCLI-proprietary film. From a comparison of the time dependence of the α's of these coated samples, relative to those of their uncoated counterparts, it is apparent that the coatings have degraded.

In order to investigate the conductive coatings themselves, assume that

$$(1 - \alpha_c) = (1 - \alpha_u)\exp[-2K(t)z] \tag{19}$$

Equation (19) gives the anticipated relation between the absorptance of the entire coated material, α_c, of the uncoated material, α_u, and the parameters of the coating (specifically, the absorption coefficient K, and the thickness z). Because of the degradation of the coating, $K(t)$ is a function of time. A general equation for this evolution is

$$K(t)z = a + \frac{bt}{365} + c\exp\left(-\frac{t}{\tau}\right) \tag{20}$$

The parameter "a," which gives the value of $K(t)z$ at $t = 0$, actually includes two effects: 1) the value of the initial absorption coefficient of the conductive coating; and 2) the change in reflectance of the material caused by the addition of the coating. Thus, "a" need not be positive.

Equations that can be fitted to the uncoated Kapton and fused-silica samples were presented above. Use of these fitted equations for α_u and the raw data of Figs. 5 and 7 for α_c permits the use of Eq. (19) to calculate the behavior of $K(t)z$ alone. Figure 8 presents the evolution of $K(t)z$ so obtained for the two coatings. The best-fit parameters to Eq. (20), along with their standard deviations and the standard error of the fit for the coatings, are listed in Table 5. We note that the OCLI coating degradation is more severe for the first three years, but later the indium-tin oxide has the greater degradation. To calculate the time dependences of the composites of the coatings and their substrates, use Eq. (19) and the appropriate equation for α_u.

Fabrics

The Astroquartz fabrics consist of woven silica fibers where the sizing used in the weaving process was removed with a high-temperature vacuum bakeout; therefore, they should be space stable. However, they both have a nonspace-stable backing (tape in one case and aluminized Teflon FEP in the other). Although these backings are partially protected from radiation damage by the overlayer of silica fibers, they can still deteriorate. Such deterioration accounts for much of the degradation of these TCCs.

Write the general equation as

$$(1 - \alpha) = r_b \exp[-2K(t)x] \tag{21}$$

in which r_b is the reflectivity of the backing (Teflon or tape), $K(t)$ is the time-dependent absorption coefficient of the fabric, and x is the thickness. Looking at Fig. 9, we see that two independent processes are at work: 1) a transient phenomenon with a time constant on the order of 200 days; and 2) a less dramatic linear behavior. It is tempting to assume that one of these processes is due to the fabric and the other is due to the backing.

We write, using Eq. (21) for guidance, the following equation for the time evolution of α:

$$\alpha = 1 - \left[A + B\exp\left(-\frac{t}{\tau}\right)\right]\left(1 - \frac{Ct}{365}\right) \tag{22}$$

Table 6 Parameters of fabrics

	A	B	C	τ	S.E.
FEP (Eq. 22)	0.742 ± 0.001	0.059 ± 0.003	0.0047 ± 0.0002	192 ± 17	2.6E-4
Tape (Eq. 22)	0.692 ± 0.002	0.135 ± 0.005	0.0092 ± 0.0003	203 ± 14	4.5E-4
FEP (Eq. 25)	0.511 ± 0.003	0.188 ± 0.009	0.030 ± 0.001	185 ± 18	2.5E-4
Tape (Eq. 25)	0.319 ± 0.011	0.455 ± 0.014	0.154 ± 0.002	261 ± 25	4.5E-4

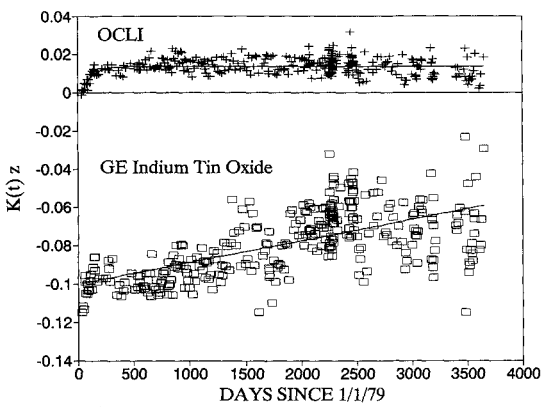

Fig. 8 Absorptance coefficient-thickness product for ITO and OCLI coatings vs time on orbit.

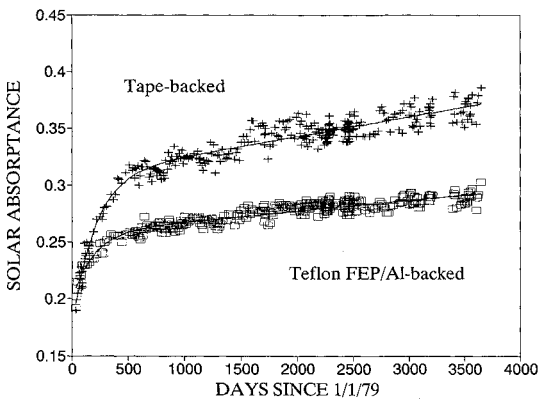

Fig. 9 Solar absorptance of FEP-backed and tape-backed silica fabric samples vs time on orbit.

In Eq. (22), the transient phenomenon is described by the parameters A, B, and τ, whereas the long-term phenomenon is controlled by C. Table 6 presents the best-fit parameters for Eq. (22).

Eq. (22) has a major theoretical deficiency. It does not predict the dependence of the absorptance of the fabric/backing composite on the absorptance of the backing alone (Ref. 14). To do so, we must include the effects of the reflectivity of the front surface, ρ, and of multiple internal reflections. We get

$$(1-\alpha) = \rho + (1-\rho)^2 y(t)[1 + \rho y(t) + \rho y(t)^2 + \cdots] \quad (23)$$

$$y(t) = r_b \exp[-2K(t)x] \quad (24)$$

Summing the infinite series, and assuming a linear and exponential time dependence for $y(t)$ as we did in Eq. (22),

$$\alpha = (1-\rho) - (1-\rho)^2 \frac{y(t)}{1-\rho y(t)} \quad (25)$$

$$y(t) = \left[A + B\exp\left(-\frac{t}{\tau}\right)\right]\left(1 - \frac{Ct}{365}\right) \quad (26)$$

By fitting Eq. (25) to the Ref. 14 data, we conclude that $\rho = 0.65$. Table 6 lists the best-fit parameters for Eq. (25), with $\rho = 0.65$ for the SCATHA data. This equation gives as good a fit as does Eq. (22).

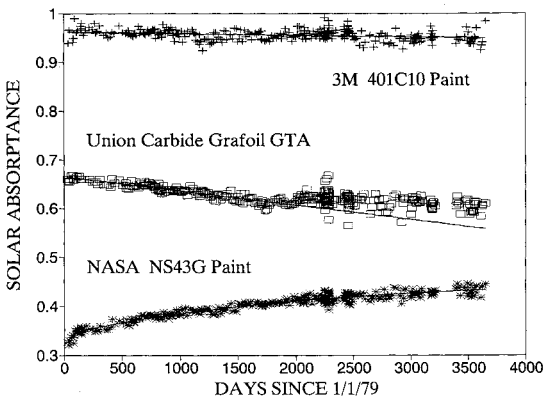

Fig. 10 Solar absorptance of tray 4 black paint, Grafoil, and yellow paint samples vs time on orbit.

Unmodeled Sample Data

In addition to the foregoing sample data, the experiment produced data for two black paint samples, a conductive yellow paint, and Grafoil. These data are plotted in Fig. 10. (The data from the black paint sample thought to have a damaged calorimeter is omitted.)

For the two black paint samples, the time evolution of α_s appears linear. Curve-fit parameters to Eq. (6) are therefore provided in Table 3 for the black paints. The negative values of Q most likely result from a radiation-caused bleaching.

The next sample under discussion is a conductive yellow paint, designated NS43G. This material exhibits degradation that is controlled by two time constants. Thus, for the fitting equation, we use

$$\alpha = \alpha_0 + a\left[1 - \exp\left(-\frac{t}{\tau_1}\right)\right] + b\left[1 - \exp\left(-\frac{t}{\tau_2}\right)\right] \quad (27)$$

The fitting parameters are $\alpha_0 = 0.312 \pm 0.004$, $a = 0.109 \pm 0.003$, $\tau_1 = 2015 \pm 195$, $b = 0.03 \pm 0.02$, $\tau_2 = 52 \pm 31$, and S.E. = 4.0E-4.

Finally, the last sample is of Grafoil. The plot of the data in Fig. 10 reveals that some sort of anomalous change has occurred at around 2000 days. Possibly, the sample experienced delamination or partial loss of adhesion with the substrate at that time. Either of these mechanisms could account for the increased scatter of data after 2000 days as the material moved about. In either case, it would be invalid to use any of the data except that between launch and 2000 days. Thus, for that time period only, we fit the data to the linear form of Eq. (6). The parameters are presented in Table 3.

Conclusions

The calorimeter experiment was carefully calibrated before launch, and initial on-orbit measurements are in good agreement with prelaunch values (with the exception of one black paint sample, where the calorimeter is probably damaged). Therefore, contamination acquired during ground calibration, testing, and launch was probably not significant, and the data may be considered truly representative of the performance of these samples at geosynchronous altitude over the 1979–89 epoch.

Metal mirrors of polished aluminum and vacuum-deposited gold, and a high-purity fused-silica second-surface silver mir-

ror, demonstrated remarkable stability in solar absorptance over 10 yr at geosynchronous altitude. This result was obtained because the rates of deposition of contaminant molecules on the samples are low. The lack of line-of-sight with other spacecraft surfaces is understood as a major factor in the low arrival rate of contamination at the samples.

Mirrors of metallized polymers showed significant growth in solar absorptance with time. Physical models of the optical darkening of polymers (based on the assumption that natural radiation is the darkening agent) have been shown to well describe the data from these samples. As discussed previously (Ref. 15), short-range particles are the cause of darkening of these samples. These could be charged particles, which are approximately isotropically distributed, or high energy photons, which are extremely directional. Because SCATHA is spinning, the exposure of these samples has been $10/\pi$ equivalent sun years.

Finally, we note that in the cases of most of the samples, it was not possible to abstract the time constant of the darkening process until many years of data were obtained. Indeed, the constants for the metal and fused-silica mirrors are still not evident. Therefore, future thermal control coating space measurement programs should contemplate lengthy data collection periods.

Acknowledgments

This work was supported by the United States Air Force Wright Laboratory (W. Ward, WL/MLBT), The Space Environmental Effects Program of the Strategic Defense Initiative Organization (M. Obal, SDIO/TNK), and the Air Force Space Systems Division under Contract F04701-88-C-0089. D. Prince, then of AFWL, helped select, characterize, and supply, most of the thermal control coating samples. Special thanks are due to the MCC-F Mission Control Team of the Air Force Consolidated Space Test Center for successfully operating P78-2 for over 10 years.

References

[1]*Description of the Space Test Program P78-2 Spacecraft and Payloads,* edited by J. R. Stevens, and A. L. Vampola, SAMSO-TR-78-24, National Technical Information Service, Springfield, MA, 1978.

[2]Fennell, J. F., "Description of P78-2 Satellite & Experiments," *The IMS Source Book,* American Geophysical Union, Washington, DC, 1982, pp. 65–81.

[3]Hall, D. F., *ML12 Spacecraft Contamination & Coatings Degradation Flight Experiment,* Air Force Wright Aeronautical Lab. TR-83-4140, Wright-Patterson AFB, OH, Dec. 1983.

[4]Hall, D. F., "Flight Experiment to Measure Contamination Enhancement by Spacecraft Charging," *Proceedings of the Society of Photo-Optical Engineers*, Vol. 216, Bellingham, WA, Feb. 4–5, 1980, pp. 131–138.

[5]Hall, D. F., *Current Flight Results From the P78-2 (SCATHA) Spacecraft Contamination and Coatings Degradation Experiment,* European Space Agency, SP-178, Paris, France, 1982, pp. 143–148.

[6]Luedke, E. E., and Kelley, L. R., *Development of Flight Units for Thermal Control Coatings Experiment,* AFML-TR-72-233, AFML/MBE, Wright-Patterson AFB, OH, 1972.

[7]Hall, D. F., and Fote, A. A., "10 Year Performance of Thermal Control Coatings at Geosynchronous Altitude," The Aerospace Corp. Rept. TOR-0090(5068-02)-1 April 1991; see also AIAA 91-1325, June 1991.

[8]Brosmer, M. A., Fischer, W. D., and Hall, D. F., "Thermal Analysis of Flight Calorimeter Instrument Designs and Calibration Test Methods," AIAA Paper 87-1622, Honolulu, HI, June 1987.

[9]Hall, D. F., and Fote, A. A., "α_s/ε_H Measurements of Thermal Control Coatings on the P78-2 (SCATHA) Spacecraft," *Heat Transfer and Thermal Control*, edited by A. L. Crosbie, Vol. 78, Progress in Astronautics and Aeronautics, AIAA, New York, 1981, pp. 467–486.

[10]Steen, P. G., *SCATHA Experiment Shadowing Study,* Systems, Science and Software, SSS-R-78-3658, La Jolla, CA, 1978.

[11]Press, W. H., Flannery, B. P., Teukolsky, S. A., and Vetterling, W. T., *Numerical Recipes,* Cambridge University Press, Cambridge, MA, 1987, p. 512.

[12]Snedecor, G. W., and Cochran, W. G., *Statistical Methods,* Iowa State Univ. Press, Ames, IA, 1967, p. 50.

[13]Stewart, T. B., Arnold, G. S., Hall, D. F., and Marten, H. D., "Absolute Rates of Vacuum-Ultraviolet Photochemical Deposition of Organic Films," *Journal of Physical Chemistry,* Vol. 93, No. 6, March 1989, pp. 2393–2400.

[14]Eagles, A. E., and Belanger, V. J., *Conductive Coatings for Satellites,* AFML-TR-76-233, Dec. 1976, p. 6.

[15]Hall, D. F., and Fote, A. A., "α_s/ε_H Measurements of Thermal Control Coatings Over Four Years at Geosynchronous Altitude," *Spacecraft and Contamination: Sources and Prevention*, edited by J. A. Roux and T. D. McCay, Vol. 91, Progress in Astronautics and Aeronautics, AIAA, New York, 1984, pp. 215–234.